iScience

Article

Transcription factor Zfx regulates tumor's evasion to T cell killing in immunotherapy

Graphical abstract

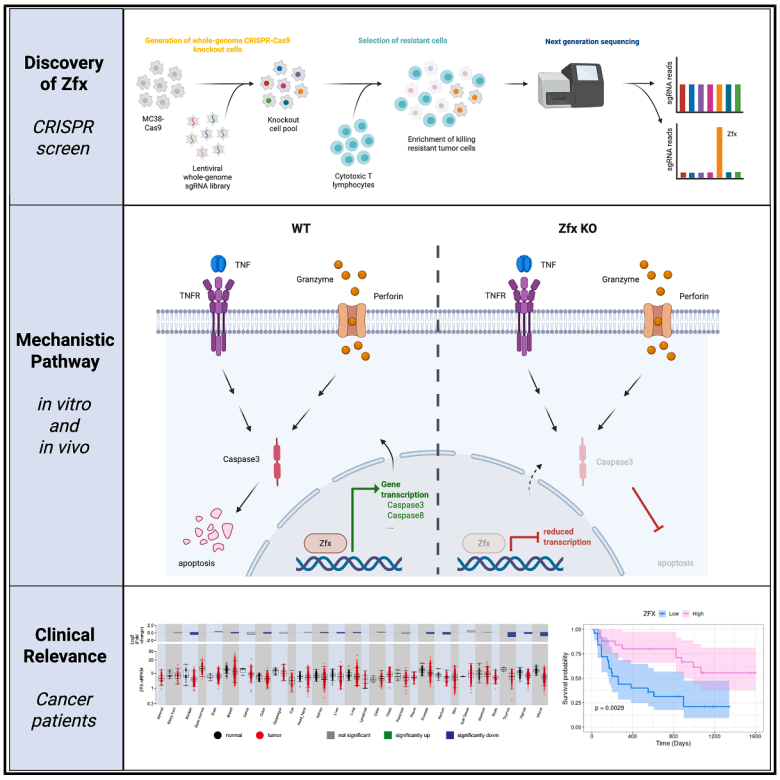

Highlights

- Genome-wide screen identifies Zfx as a novel regulator of tumor immune evasion
- The transcription factor Zfx directly controls cell death pathway genes
- Zfx knockout protects tumor cells from T cell-mediated killing
- ZFX expression is a biomarker for cancer immunotherapy response

Authors

Ulrike Kaufmann, Joy Wang, Marinella G. Callow, ..., Scott Martin, Mike Costa, Haochu Huang

Correspondence

kaufmann.ulrike@gene.com

In brief

Oncology

Kaufmann et al., 2025, iScience 28, 113842
November 21, 2025
https://doi.org/10.1016/j.isci.2025.113842

CellPress

iScience

CellPress
OPEN ACCESS

Article

Transcription factor Zfx regulates tumor's evasion to T cell killing in immunotherapy

Ulrike Kaufmann,[1,9,*] Joy Wang,[1] Marinella G. Callow,[2] Jean-Philippe Fortin,[3] Szymon Myrta,[4] Dorothee Nickles,[5] Rohit Reja,[5] Eric Cheng,[1] Erin Wonder,[1] Benjamin Haley,[6] Yuxin Liang,[7] Scott Martin,[2] Mike Costa,[2] and Haochu Huang[1,8]

[1]Department of Translational Oncology, Genentech Inc., South San Francisco, CA, USA
[2]Department of Research Oncology, Genentech Inc., South San Francisco, CA, USA
[3]Department of Bioinformatics, Genentech Inc., South San Francisco, CA, USA
[4]Roche Global IT Solution Center, Genentech Inc., South San Francisco, CA, USA
[5]Oncology Bioinformatics, Genentech Inc., South San Francisco, CA, USA
[6]Molecular Biology, Genentech Inc., South San Francisco, CA, USA
[7]Next Generation Sequencing and Proteomics, Genentech Inc., South San Francisco, CA, USA
[8]Senior author
[9]Lead contact
*Correspondence: kaufmann.ulrike@gene.com
https://doi.org/10.1016/j.isci.2025.113842

SUMMARY

Cancer immunotherapy aims to boost T cell responses against tumor cells. However, a large fraction of patients with cancer exhibit intrinsic or acquired resistance to immunotherapy. To better understand resistance mechanisms in tumor cells, we used CRISPR-Cas9 whole-genome screening to uncover tumor-specific genes that influence sensitivity to T cell killing. Among the top hits, we identified the transcription factor zinc-finger protein X-linked (Zfx). Zfx knockout tumor cells are resistant to T cell killing both *in vitro* and *in vivo*. We demonstrate that Zfx regulates expression of the apoptotic machinery, with Caspase-3 being a central element in mediating T cell killing. Mechanistically, our ChIP-Seq analyses in multiple human cancer cell lines show ZFX directly binds to the promoters of key apoptosis genes, including Caspase-3, to control their expression. Notably, ZFX expression is decreased in several human cancer tissues compared to healthy tissues. Female patients with kidney renal clear cell carcinoma (KIRC) with high ZFX expression showed longer survival compared to patients with low ZFX expression. In addition, we find that higher ZFX expression in patients with melanoma correlates with a positive response to anti-PD-1 immunotherapy. Our results demonstrate a novel resistant mechanism in tumor cells, highlighting ZFX as a potential biomarker for immunotherapy response, and suggest that targeting tumor cell intrinsic resistance genes in combination with immune therapies could benefit patients with cancer.

INTRODUCTION

Efficient control of tumor growth by the immune system depends on a series of steps known as the cancer-immunity cycle.[1] In brief, the uptake of dead and dying tumor cells by dendritic cells leads to the presentation of tumor neoantigens to T cells, resulting in their priming and activation. This enables T cell trafficking to tumors, where they kill antigen-specific tumor cells, thereby initiating the cycle again. Each step is tightly controlled and necessary for an effective anti-tumor immune response. Several immunotherapies are already available or under investigation to support the cancer-immunity cycle, particularly anti-CTLA4 for priming and activating T cells and anti-PD-1/PD-L1 for killing of tumor cells.[2–5] Despite the clinical success of immunotherapies, significant challenges remain.[6–8] Many patients do not benefit durably from checkpoint blockade and show an intrinsic or adaptive resistance to the anti-cancer immune response.[9–11] Most clinical strategies focus on improving the cytotoxicity of T cells without considering tumor intrinsic resistance factors. It is critical to understand the mechanisms responsible for tumor cell resistance in order to address the need for better treatment options. Combining immune cell-focused approaches with increasing tumor intrinsic sensitivity to death signals may improve cancer patient outcomes.

To better understand tumor-intrinsic resistance to T cell killing, a whole-genome CRISPR-Cas9 screen was performed to systematically uncover novel tumor resistance genes in an unbiased manner. Similar approaches have been used successfully to study tumor and T cell interactions in recent years.[12–16] Whereas the importance of antigen presentation as well as cytokine signaling was well established by these screens, factors regulating resistance to T cell-mediated killing are not completely understood. To specifically focus on discovering novel resistance mechanisms in tumor cells, it is necessary to use a tumor cell line that is sensitive to T cell-mediated killing *in vitro* and responsive to checkpoint blockade therapy *in vivo*. Therefore, the

mouse colorectal cancer cell line MC38 was chosen as it is sensitive to T cell mediated-killing and, when grown *in vivo*, is responsive to checkpoint inhibition, such as anti-PD-L1.[17] Our CRISPR-Cas9 *in vitro* resistance screen with MC38 tumor cells and cytotoxic T lymphocytes revealed transcription factor Zfx as a novel regulator of apoptosis pathways in tumor cells and caspase-3 is one of the central components regulated by Zfx.

RESULTS

Whole-genome CRISPR-Cas9 resistance screen in MC38 tumor cells uncovers regulators of the apoptosis pathway

To identify tumor intrinsic genes that are involved in killing resistance, we performed a pooled whole-genome CRISPR-Cas9 knockout resistance screen in MC38 tumor cells co-cultured with cytotoxic T cells *in vitro* (Figure 1A). Cas9-expressing MC38 cells were utilized in a whole-genome CRISPR-Cas9 screen (~160,000 sgRNAs) wherein cells were infected and collected as ''reference control,'' expanded as ''input control,'' pulsed with the SIINFEKL peptide, and co-cultured with OT-I transgenic T cells for the killing assay (see Figure 1A and STAR Methods). Similar to other killing assays, a higher T cell to tumor cell ratio results in more efficient killing of tumor cells. We chose a 1:1 T cell to tumor cell ratio, at which approximately 80% of tumor cells underwent cell death during the co-culture. These cells were expanded for additional rounds of killing to further enrich resistant tumor cells (Figure 1B). As T cell-mediated tumor cell killing is inefficient, false positivity for some sgRNAs may occur. However, the spurious nature of this effect can be mitigated through the use of multiple, unique gene-specific sgRNAs (here, approximately 8 sgRNAs per gene). Killing-resistant tumor cells were collected after successive rounds of culture with cytotoxic T cells, and this was followed by the amplification and sequencing of the tumor cell-integrated sgRNAs. Comparing the sgRNA representation between ''input control'' vs. ''reference control'' showed the dropout of essential genes, providing technical validation of our screen (Figure S1B). Hits were identified based on sgRNA representation fold change after the second round of killing, compared to input, with at least 3 out of 8 sgRNAs targeting one gene showing a larger than 2-fold change (Figure S1C). Examples of single guide enrichments after each round of killing are shown in Figure S1D. Among the top hits are well-characterized genes associated with cell death pathways, for example, Tnfrsf1a, Fadd, and Casp8 (Figure 1C). Interestingly, members of the antigen presentation complex, such as B2m, were not among the hits (Figure S1D), which is a known mechanism of tumor immune evasion.[18] Pathway analysis linked the screening hits to apoptosis and TNFa signaling pathways, amongst others (Figure 1D).

TNFa-mediated killing is the dominant killing mechanism in MC38 tumor cells *in vitro*

To further validate the screening results, and particularly the involvement of the TNFa signaling pathway, recombinant TNFa was tested for MC38 tumor cell killing. Titration studies with recombinant murine TNFa showed that MC38 tumor cells are sensitive to TNFa-mediated killing (Figure 1E). To confirm that TNFa is responsible for killing MC38 tumor cells in the T cell-tumor cell co-culture, supernatant from the co-culture was added to fresh MC38 cells and resulting in equivalent killing as activated OT-1 T cells (Figure 1F). The amount of TNFa present in the supernatant was measured by ELISA. The detected concentration of about 3 ng/mL (Figure 1G) is consistent with the concentrations used in the recombinant TNFa titration experiment (Figure 1E).

We next investigated whether TNFa is essential for MC38 tumor cell killing by OT-1 T cells. For these studies, we used a TNFa -neutralizing antibody, which was added to either recombinant TNFa-mediated or OT-1 T cell-mediated killing assays. As expected, TNFa-neutralizing antibody blocked TNFa induced cell death. Interestingly, blocking TNFa also inhibited the killing of MC38 tumor cells by OT-1 T cells (Figure 1H). To confirm that the OT-1 T cells are capable of producing cytotoxic effector molecules in addition to TNFa, we analyzed the expression of IFNg, TNFa, and Granzyme B, as well as the degranulation marker CD107a, by flow cytometry. OT-1 T cells expressed high levels of INFg, TNFa, and CD107a in the presence of SIINFEKL peptide (Figure 1I). Granzyme B levels were found to be lower in peptide-stimulated T cells compared to the unstimulated control. This observation suggests that Granzyme B is released upon stimulation. To further characterize the functionality of these T cells we tested their killing efficiency in E0771 cells. Strong killing of EO771 cells even in the presence of TNFα-neutralizing antibodies (Figure S2B), indicates the presence and functionality of other cytotoxic agents, such as Granzyme B, besides TNFα (Figure S2B). This clearly indicates that the MC38 tumor cells were exposed to adequate levels of Perforin and Granzyme B necessary for effective *in vitro* tumor cell killing. However, Figure 1H shows that neutralizing TNFα in the presence of Granzyme B and Perforin results in 80% survival of Zfx knockout (KO) tumor cells. This suggests that Zfx KO tumor cells are protected from TNFα-induced cell death.

Collectively, these results show that MC38 tumor cells are sensitive to TNFa-mediated cell death, and moreover, TNFa is the dominant mechanism of how antigen-specific T cells kill MC38 cells *in vitro*. For comparison, we examined several commonly used murine tumor cell lines for their sensitivity to TNFa. Most cell lines were not sensitive to TNFa (Figure S2A). E0771 is partially sensitive to TNFa-mediated killing, and as a consequence, neutralizing TNFa showed a smaller effect on OT-1 T cell-mediated killing of E0771 (Figure S2B). Furthermore, we performed supernatant killing experiments with E0771 cells, which showed no sensitivity to killing when supernatants from activated T cell assays were added. This emphasizes that the TNF-α sensitivity is a distinctive characteristic of MC38 tumor cells (Figure S2C).

Loss of zinc-finger protein X-linked results in resistance to T cell-mediated killing of tumor cells

Among the top screening hits was the novel finding of the transcription factor Zinc Finger Protein X-linked (Zfx) (Figure 1C). To validate the effects of Zfx disruption, MC38 clones were generated and used to make Zfx KO clones using Cas9-RNP. Zfx knockout was validated by NGS and revealed a large deletion and frameshift mutation in two of the clones used throughout this article (Figure 2A). Both deletions are within the

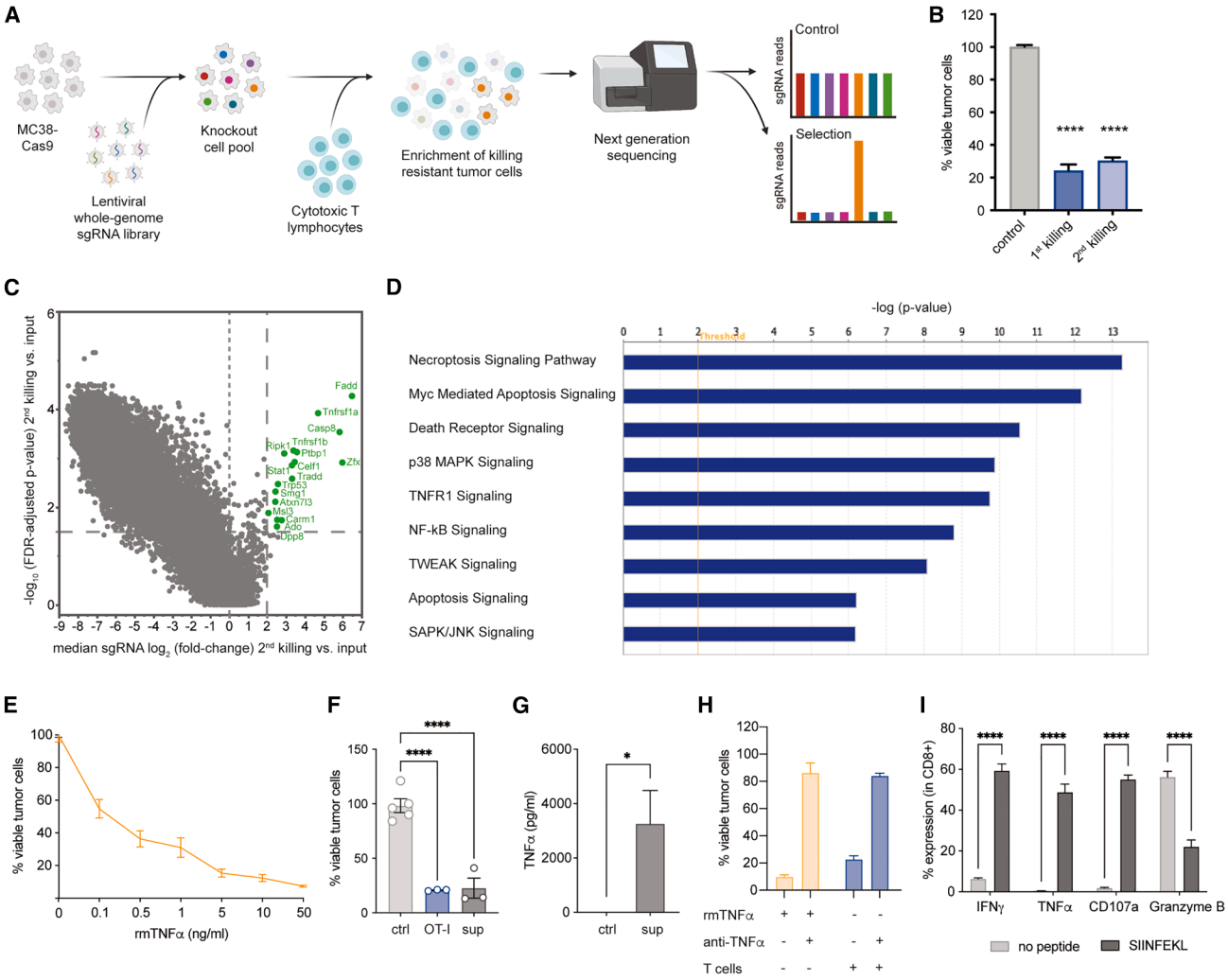

Figure 1. Whole-genome CRISPR Cas9 screen reveals cell death signaling pathways among dominant hits

(A) Schematic overview of CRISPR-Cas9 knockout screen in MC38 tumor cells co-cultured with cytotoxic T lymphocytes.

(B) Viability readout of tumor cells after the first and second rounds of killing with cytotoxic T cells co-cultured for 5 h with peptide loaded tumor cells. Control tumor cells were not loaded with the peptide. Viability was measured with the ViCell counter after 24 h. Error bars indicate SEM of 3 replicates for each of the 4 sub-libraries containing the whole-genome library. Statistics with Welch's t test ****$p < 0.0001$.

(C) Volcano plot of $\log_2$ fold-change versus p-value of the second round of killing versus input. Fry gene-level statistics with $\log_2$ fold-change >2 and FDR-adjusted p-value $-\log_{10} > 1.5$.

(D) Most significant pathways by Ingenuity Pathway Analysis ($p < 0.05$) from top candidates of CRISPR screen.

(E) TNFa-mediated killing of MC38 tumor cells treated overnight with increasing concentrations of recombinant murine TNFa. Viability of tumor cells was assessed with CellTiter-Glo. Shown are $n = 6$ samples per group and error bars indicate SEM.

(F) Killing assay with T cells and supernatant from co-cultured tumor and T cells. Viability readout of tumor cells with CellTiter-Glo after overnight incubation. Dots represent individual measurements of $n = 3$ samples, and error bars indicate SEM. Statistics with one-way ANOVA: ****$p < 0.0001$.

(G) Detection of TNFa in supernatant of co-cultured tumor and T cells by ELISA. Control without T cells. $N = 2$ samples in triplicate. Error bars indicate SEM. Statistics with Welch's t test: *$p < 0.05$.

(H) Cytotoxicity assay: MC38 tumor cells were either mediated through rmTNF or OT-I T cells treated with neutralizing TNFa antibodies. Viability of tumor cells was measured with CellTiter-Glo after overnight incubation. Bar graphs show the mean of $n = 6$ samples per group and error bars indicate SEM.

(I) OT-I T cells were co-cultured with or without SIINFEKL peptide loaded tumor cells. Expression of cytotoxicity makers (IFNg, TNFa, CD107a, and Granzyme B) was detected by flow cytometry. Representative flow cytometry plots gated on CD8 positive T cells on the right. Quantitative data shown (left) are means of $n = 7$ samples per group, and error bars indicate SEM. Statistics with one-way ANOVA: ****$p < 0.0001$.

transcriptional activation domain of Zfx, resulting in a truncated protein. MC38-Zfx KO clones showed no significant difference to the MC38-WT clone with respect to cell proliferation, MHC-I expression, and peptide presentation (Figures 2B and 2C). This comparison was conducted to confirm that MHC-I is not down-regulated in Zfx-KO cells. Therefore, the observed resistance to cytotoxic killing in these cells cannot be attributed to reduced MHC-I expression or impaired antigen presentation.

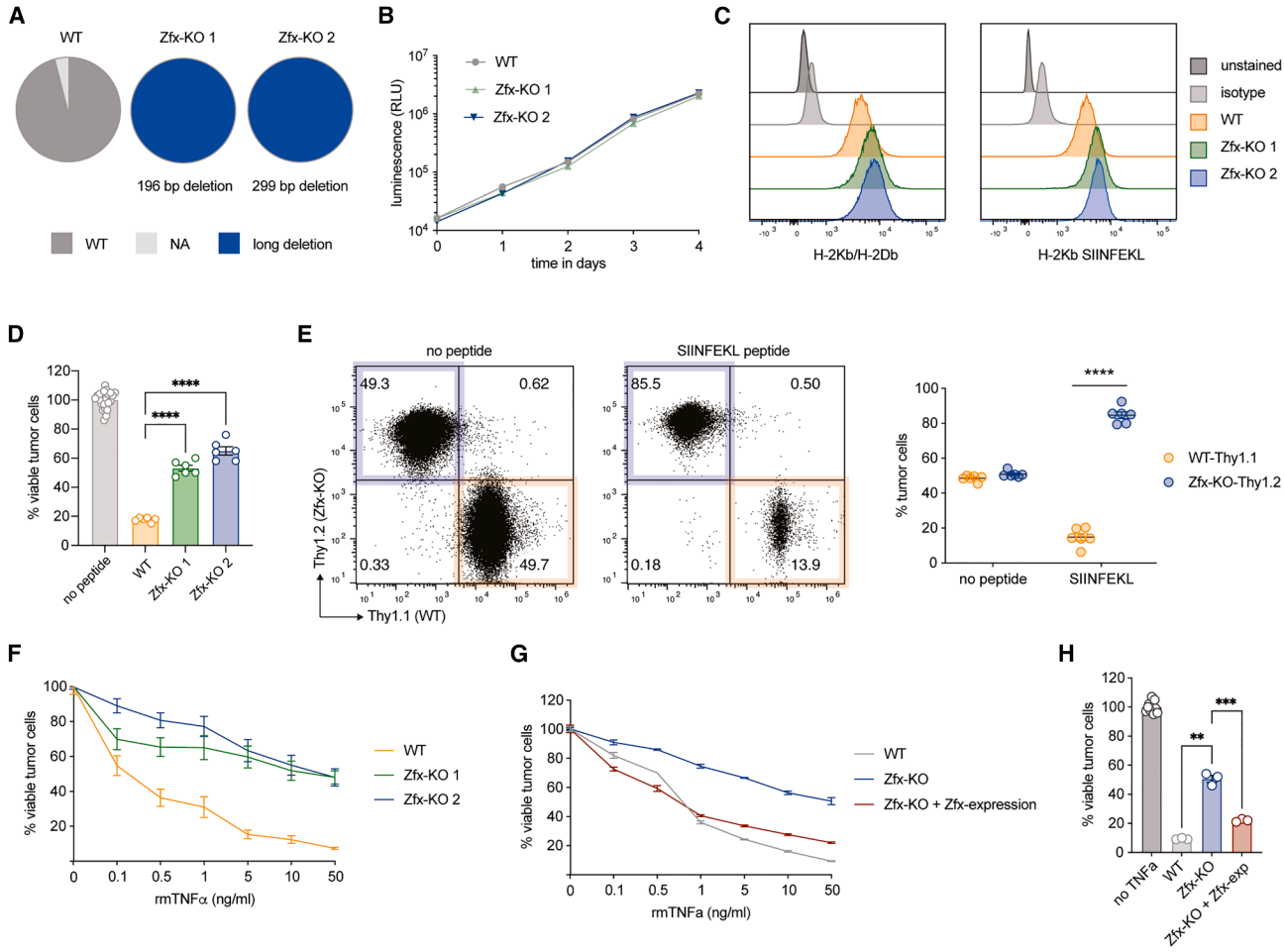

Figure 2. Zfx loss results in increased resistance to T cell-mediated killing *in vitro*

(A) Genotyping results by next generation sequencing of WT and Zfx KO MC38 clones generated with CRISPR RNP and 2 sgRNA targeting Zfx to induce large deletions. The wildtype sequence is indicated in dark gray, and the long deletion mutation is shown in blue.

(B) Proliferation of WT and Zfx KO MC38 tumor cells over 4 days. Viable cell numbers detected with CellTiter-Glo.

(C) MHC-I expression (stained with H-2Kb/H-2Db antibody) and SIINFEKL peptide loading (stained with H-2Kb SIINFEKL antibody) of WT and Zfx KO MC38 tumor cells. Representative flow cytometry plots.

(D) Cytotoxicity assay with WT and Zfx KO tumor cells loaded with SIINFEKL peptide and co-cultured with activated OT-I transgenic T cells. Viable tumor cells detected with CellTiter-Glo. Dots represent individual measurements of $n = 6$ samples, and error bars indicate SEM. Statistics with Welch's t test: ****$p < 0.0001$.

(E) Competition assay of WT (Thy1.1) and Zfx KO (Thy1.2) MC38 tumor cells loaded with SIINFEKL peptide and co-cultured with activated OT-I transgenic T cells. Representative flow cytometry analysis (left) and quantification of $n = 6$ samples (right). Dots represent individual measurements, and error bars indicate SEM. Statistics with unpaired t test: ****$p < 0.0001$.

(F) TNFa-mediated killing of MC38 WT and Zfx KO tumor cells treated overnight with increasing concentrations of recombinant murine TNFa. Viability of tumor cells was assessed with CellTiter-Glo. Shown are n = 5–6 samples per group and error bars indicate SEM.

(G and H) MC38 Zfx-KO tumor cells were engineered to overexpress Zfx. WT, Zfx-KO, and Zfx-KO + Zfx over-expressing cells were treated with increasing concentrations of rm TNFa overnight. Viable tumor cells were detected with the CellTiter-Glo assay and normalized to no TNFa treatment. Titration of rm TNFa (G) and bar graphs at 50 ng/mL TNFa (H). Graphs show mean, and error bars indicate SEM of $n = 3$ samples per group. Statistics with Welch's t test: ***$p < 0.0005$.

A T cell-mediated cytotoxicity assay confirmed the significant resistance to T cell-mediated killing in Zfx KO tumor cells compared to WT (Figure 2D). Moreover, we repeated the *in vitro* T cell killing assay with mixed WT and Zfx KO cells to test whether resistance to T cell-mediated killing is intrinsic to Zfx KO. The results showed that Zfx KO tumor cells were strongly selected against WT tumor cells during T cell-mediated killing, resulting in a 6-fold higher frequency of Zfx KO cells (Figure 2E). Zfx KO tumor cells exhibit resistance not only to T cell-mediated killing, but also to killing mediated solely by recombinant TNFa (Figure 2F). In addition, to rule out putative off-target effects of CRISPR in Zfx KO cells, we performed a rescue experiment. When Zfx was overexpressed in Zfx KO tumor cells, the cells became sensitive to TNFa- and T cell-mediated killing (Figures 2G and 2H). Collectively, these data confirm that Zfx regulates tumor cell death mediated by T cells.

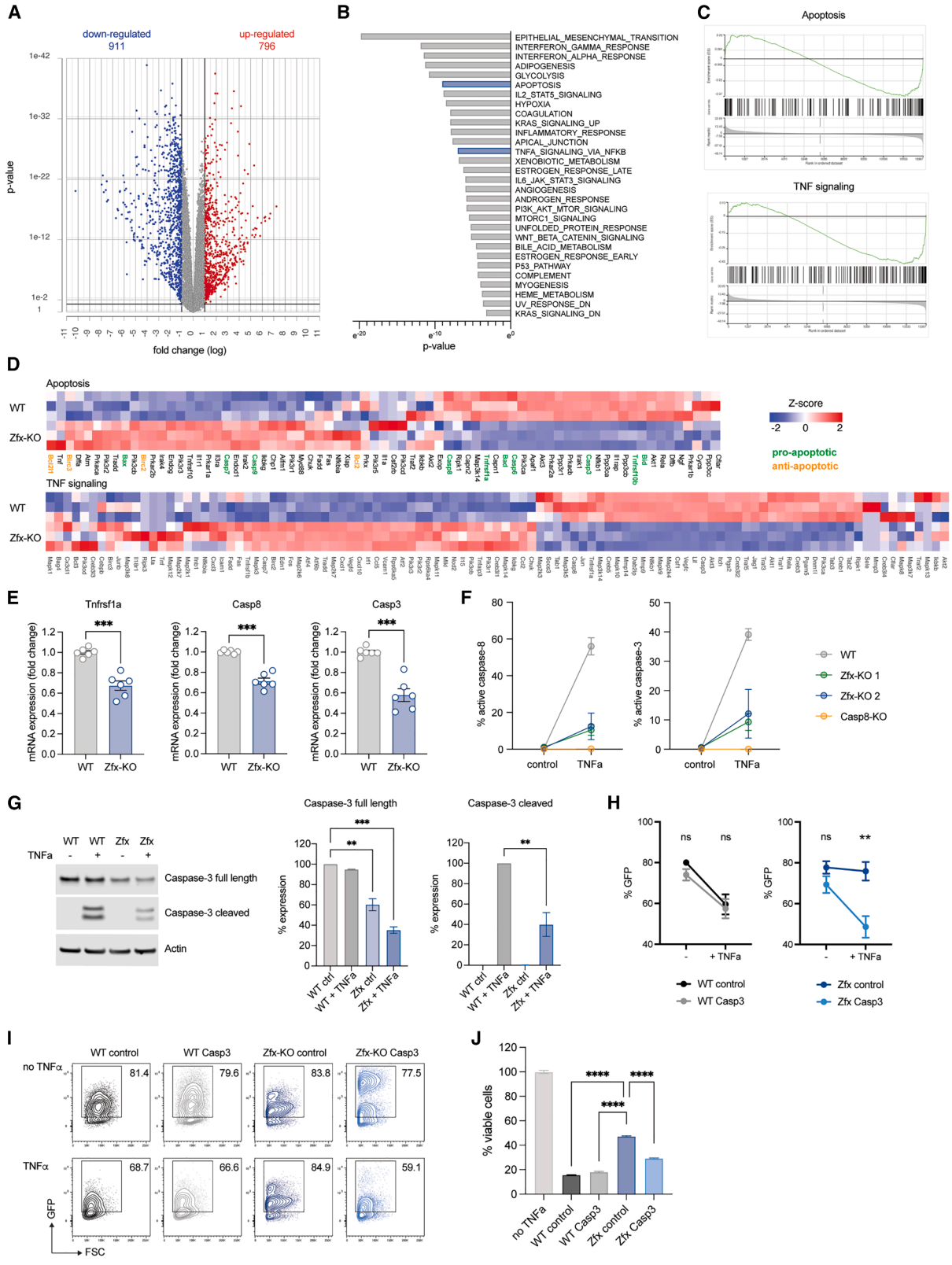

(legend on next page)

Zfx regulates the expression of genes associated with apoptosis and TNFa signaling pathways

To investigate the mechanisms by which Zfx regulates tumor cells' sensitivity to T cell-mediated killing, we compared the transcriptomes of WT and Zfx KO tumor cells. Bulk mRNA sequencing identified 1707 differentially expressed genes, of which 911 genes were downregulated and 796 genes were upregulated in Zfx KO tumor cells compared to WT cells (Figure 3A, Table S2). Pathway analysis with MSigDB's Hallmark dataset[19] showed apoptosis and TNFa signaling pathways among the most enriched pathways (Figures 3B and 3C, Sup Table). Several pro-apoptotic genes were downregulated in the Zfx KO tumor cells, such as Casp3, Casp6, Casp8, Bid, Bad, Tnfrsf1a, and Tnfrsf10b, whereas a number of anti-apoptotic genes were upregulated in the Zfx KO tumor cells, for example, Bcl2l1, Bcl2, Birc2, and Birc3 (Figure 3D). Based on these observations, we hypothesize that Zfx regulates the expression of key genes important for apoptosis and cell death, and as a consequence, loss of Zfx results in resistance to induced cell death.

Next, we validated the RNA-seq results with quantitative real-time PCRs (qRT-PCR), confirming the reduced expression of Tnfrsf1a, Casp3 and Casp8 in Zfx KO tumor cells (Figure 3E). Furthermore, we used a staining assay for active Caspase 3 and 8 (Figure 3F). TNFa strongly induced the generation of active Casp8 and Casp3 in WT tumor cells. Both active Casp3 and Casp8 were significantly reduced in TNFa-treated Zfx KO compared to WT tumor cells, indicating a defect in extrinsic apoptosis signaling. In contrast, Casp8 KO tumor cells showed neither active Casp8 nor active Casp3, confirming that the active caspase staining was specific (Figure 3F). In addition, Western blots confirmed decreased expression of both Casp3 protein (full length) and active Casp3 (cleaved) in TNFa-treated Zfx-KO cells (Figure 3G).

Casp3 overexpression restores zinc-finger protein X-linked knockout tumor cells' sensitivity to TNFa

Our results support the hypothesis that Zfx regulates the expression of key genes important for apoptosis and cell death. Given that various cell death pathways converge on Casp3 activation and that Casp3 activation was decreased in Zfx KO tumor cells, we asked whether increasing Casp3 expression is sufficient to restore the tumor cells' sensitivity to TNFa in Zfx KO cells. To this end, we generated Zfx KO and WT cell lines that stably expressed a Tet-inducible Casp3-IRES-GFP (Zfx-KO Casp3 or WT Casp3) or GFP alone (Zfx-KO control, WT control), respectively. This approach allowed us to use GFP expression as a surrogate marker of Casp3 expression and to enrich GFP+ cells by flow. While there was a reduction of GFP+ cells in the WT setting after TNFa treatment, there was no significant difference between control and Casp3 overexpressing cells, suggesting that overexpression of Casp3 itself does not induce or enhance cell death. In contrast, in Zfx KO cells, overexpressing Casp3 but not GFP alone resulted in significantly lower frequency of GFP+ cells after TNFa treatment, confirming that Casp3 partially restored the cells' sensitivity to TNFa (Figure 3H). Interestingly, cells expressing high levels of GFP, and therefore Casp3, showed the most sensitivity to TNFa (Figure 3I). We also confirmed this result by quantifying the frequencies of viable cells by CellTiter-Glo assay, which is independent of GFP expression (Figure 3J).

Zinc-finger protein X-linked knockout MC38 tumor cells are resistant to immunotherapy

Next, we investigated the role of Zfx loss in MC38 tumors *in vivo* in response to immunotherapy. We engineered MC38 WT and Zfx KO tumor cells to express Thy1.1 or Thy1.2 stably, so we could track them easily with flow cytometry when they were mixed together. First, C57BL/6 mice were inoculated with a 1:1 mixture of MC38-WT-Thy1.1 and MC38-Zfx-KO-Thy1.2 tumor cells. After tumors reached 120–200 mm^3, mice were grouped out and treated with anti-PD-L1 or anti-gp120 isotype control (Figure 4A). At day 7 of treatment, tumor volume and tumor weight of anti-PD-L1 treated mice were significantly reduced, indicating that the treatment was efficacious (Figures 4B and 4C). Increased frequency of tumor-infiltrating CD8 T cells, as well as decreased frequency of exhausted ($PD\text{-}1^+$ $Tim3^+$) CD8 T cells, further confirmed the effectiveness of anti-PD-L1 treatment (Figure 4D). Interestingly, comparison of WT and Zfx KO tumor cell ratios revealed a dominance of Zfx KO tumor cells over WT tumor cells in the anti-PD-L1 treated group, demonstrating their resistance against T cell-mediated killing *in vivo* (Figure 4E). No difference was detected in isotype control treated

Figure 3. Zfx loss impairs the expression of multiple genes associated with apoptosis

(A–D) RNA sequencing of WT and Zfx KO MC38 tumor cells from *in vitro* cell culture.

(A) Volcano plot of up- and down-regulated genes with a threshold of 2-fold-change and p-value <0.05.

(B) Hallmark pathway analysis of genes with significant expression changes.

(C) Gene set enrichment analysis for apoptosis and TNF signaling pathway.

(D) Heatmap of apoptosis and TNF signaling pathway (KEGG).

(E) Quantitative real-time PCR for WT and Zfx KO MC38 tumor cells. Statistics with Welch's t test: $^{***}p < 0.001$.

(F) Percentage of WT and Zfx KO MC38 tumor cells stimulated with recombinant murine TNFa with active Caspase-8 and Caspase-3, assessed by flow cytometry with CaspGlow kit. Caspase-8 KO cells served as a negative control. Error bars indicate SEM of $n = 2$ samples.

(G) Western Blot of WT and Zfx KO MC38 tumor cells stimulated with or without recombinant murine TNFa. Quantification of $n = 3$ independent experiments with error bars indicating SEM. Statistics with one-way ANOVA: $^{***}p < 0.001$ and $^{**}p < 0.01$.

(H and I) WT and Zfx KO MC38 tumor cells with induced expression of control or Caspase-3 overexpression vector were treated with and without TNFa for 24 h. Frequency of GFP expression was measured by flow cytometry and quantified for $n = 3$ independent experiments with error bars indicating SEM. Statistics with two-way ANOVA: $^{**}p < 0.01$.

(J) Cells from H and I were used for TNFa-mediated killing assays. FACS sorted GFP+ cells were treated overnight with recombinant murine TNFa. Viability of tumor cells was assessed with CellTiter-Glo. Shown are $n = 3$ samples per group in triplicate, and error bars indicate SEM. Statistics with one-way ANOVA: $^{****}p < 0.0001$.

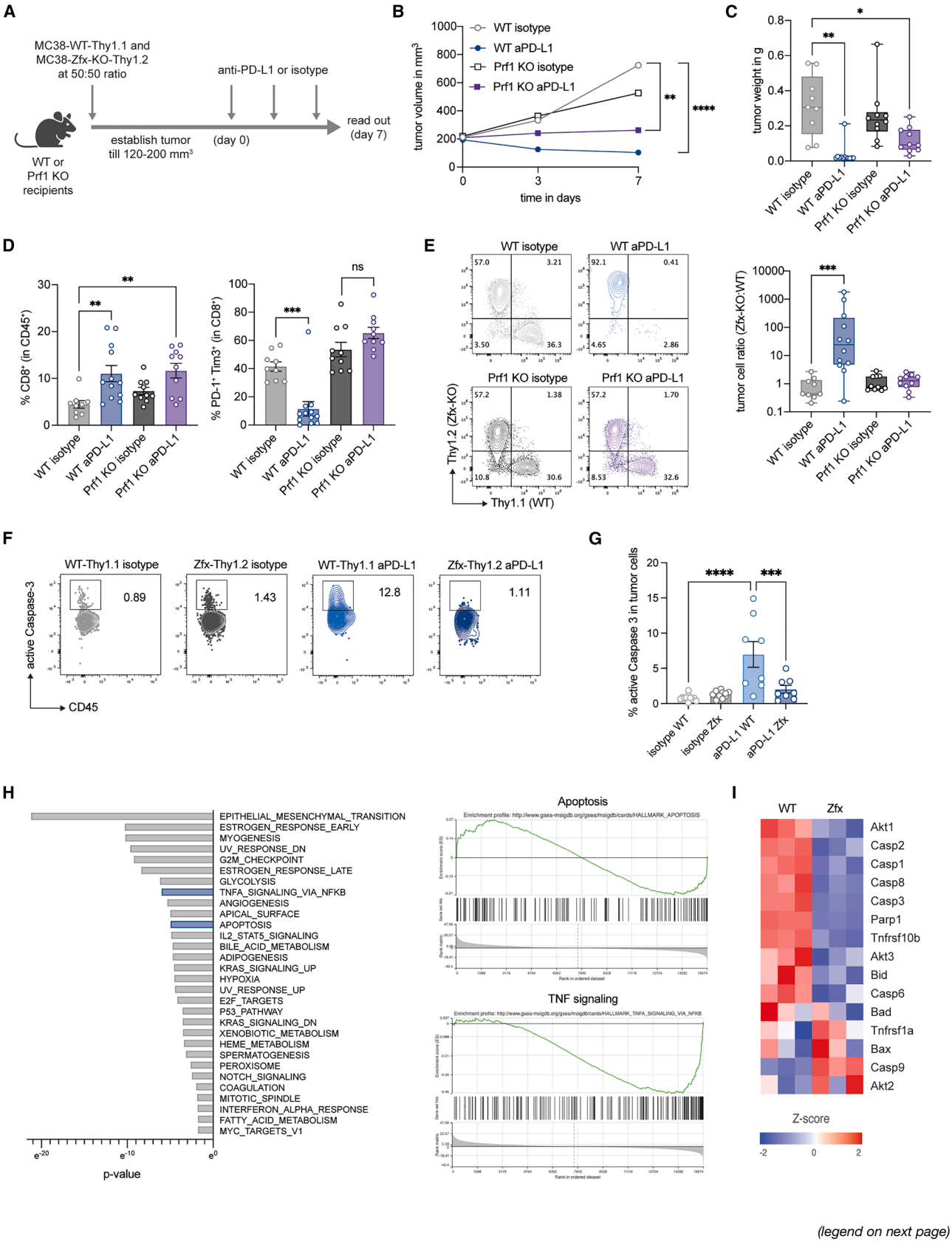

(legend on next page)

mice, suggesting that the dominance of Zfx KO tumor cells is only apparent when a strong immune response against tumor cells is present.

To further examine the killing mechanism involved in this resistance, we repeated the study with Perforin KO mice. As described previously[17] Perforin KO mice showed a limited response to anti-PD-L1 treatment, demonstrated by a moderate impact on tumor volume and weight (Figures 4B and 4C). In keeping with the role for Zfx to mediate MC38 cell sensitivity to T cell-mediated killing, the dominance of Zfx KO tumor cells was completely lost in Perforin KO mice treated with anti-PD-L1 (Figure 4E). These results demonstrated that Zfx regulates cell death induced by the Perforin and Granzyme B pathway *in vivo,* which is in contrast to the results of our *in vitro* studies, which suggest that TNFa is the major mechanism killing MC38 cells. To further clarify the role of TNFa pathway *in vivo*, we generated TNFR1 KO MC38 cells and compared them to WT MC38 cells that express Ovalbumin (OVA). We decided to use this model system here to closely resemble the *in vitro* MC38 killing assay and screen, in which OT-I-specific T cells were used. We first validated the TNFR1 KO *in vitro*. To this end, we performed two rounds of killing with OT-I T cells and detected increased killing resistance in TNFR1 KO tumor cells, especially after the second round of killing (Figure S4A). In addition, the frequency of TNFR1 KO was assessed by NGS of the tumor cell lines before and after each round of killing. NGS revealed TNFR1 KO in about 50% of tumor cells before killing and an increase to >98% after two rounds of T cell mediated killing (Figure S4B). Next, we performed *in vivo* studies with NSG mice inoculated with MC38-WT-Thy1.2-OVA and MC38-TNFR1-KO-Thy1.1-OVA tumor cells separately or mixed. OT-I T cells for tumor-specific killing were transferred at day 7 after tumor inoculation, and tumors were monitored until day 28, and tumor tissues were analyzed on day 18 (Figure S1C). Tumor growth indicated that both WT and TNFR1 KO tumors grew similarly when no OT-I T cells were transferred (Figure S4D). After OT-I T cell transfer, both tumor types showed strongly reduced tumor growth, but surprisingly, no significant difference, indicating no resistance in the TNFR1 KO tumor inoculated mice to T cell-mediated killing *in vivo* (Figure S4D). To further confirm the relative resistance to T cell killing, we performed mixed tumor studies. Interestingly, mixed tumor studies revealed an increased frequency of TNFR1 KO tumor cells both with and without OT-I T cell transfer, indicating TNFR1 KO tumor cells have survival advantages *in vivo* (Figure S4E). Most likely, this effect takes place right after the inoculation of tumor cells, before T cells are transferred, and thus is seen in both groups with and without T cell transfer. Regarding the source of TNFa, it is most likely coming from macrophages that are present in NSG mice[20] (Behan 2013 Obesity). After OT-I transfer, overall tumor cell growth was dramatically suppressed. However, it did not affect the enrichment of TNFR1 KO tumor cells significantly when compared to the case without OT-I transfer, suggesting that TNFR1 KO did not offer resistance to T cell killing. This is quite different from the dramatic enrichment of Zfx KO cells.

Since we identified Caspase-3 as a key target of Zfx *in vitro* (Figure 3) and the Perforin/Granzyme pathway could activate Casp3, we investigated Casp3 activation *in vivo*. WT-Thy1.1 and Zfx KO-thy1.2 tumor cells isolated from the same tumors were stained with an active Caspase-3 detection antibody. Active Caspase-3 was significantly increased in WT tumor cells after anti-PD-L1 treatment, in contrast to anti-PD-L1 treated Zfx KO tumor cells, whose active Caspase-3 levels were comparable to isotype control treated groups (Figures 4F and 4G). To examine the transcriptomes of tumor cells *in vivo*, we performed RNA sequencing from *ex vivo* isolated WT and Zfx KO tumor cells from the same mice and FACS sorted for WT-Thy1.1 and Zfx-KO-Thy1.2. Gene set enrichment analysis indicated apoptosis and TNFa signaling pathways as deregulated in Zfx KO tumor cells (Figure 4H), similar to our *in vitro* data. Selected genes with important roles in the apoptosis pathways were downregulated in Zfx KO tumor cells, e.g., Casp1, Casp2, Casp3, Casp6, and Casp8 (Figure 4I).

Taken together, Zfx plays an important role in MC38 tumors *in vivo*. Zfx regulates the expression of apoptosis pathway members, especially Caspase-3, and thus results in increased resistance to T cell-mediated killing *in vivo*. Since Caspase-3 is downstream of Perforin and Granzyme B induced killing, the regulation of Caspase-3 expression by Zfx explains the killing resistance of Zfx KO tumor cells *in vivo*.

Figure 4. Killing resistance of Zfx KO MC38 tumor cells is dependent on the Perforin/Granzyme B pathway *in vivo*

(A) Schematic overview of *in vivo* studies to investigate the role of Zfx KO in MC38 tumors.

(B–E) C57BL/6 or Perforin KO mice were inoculated with a 50:50 mixture of WT-Thy1.1 and Zfx-KO-Thy1.2 MC38 tumor cells. After tumors were established at 120–200 mm^3, mice were grouped and treated with anti-PD-L1 or isotype control for 7 days. Quantification of n = 9–12 mice per group from 2 independent studies. Graph shows the mean and the error bars indicate SEM. Statistics with Welch ANOVA: $^{**}p < 0.005$, $^{***}p < 0.001$, $^{****}p < 0.0001$.

(B) Tumor volume during 7-day anti-PD-L1 treatment.

(C) Tumor weight at day 7 after anti-PD-L1 treatment start.

(D) Tumor infiltrating lymphocytes were analyzed at day 7 of anti-PD-L1 treatment. Frequencies of $CD8^+$ T cells and $PD\text{-}1^+$ $Tim3^+$ $CD8^+$ exhausted T cells are quantified.

(E) Presence of WT-Thy1.1 and Zfx-KO-Thy1.2 tumor cells among gated $CD45^-$ cells isolated from tumor tissues at day 7 of anti-PD-L1 treatment. Representative flow cytometry plots on the left and quantification of Zfx-KO to WT tumor cell ratio on the right. Statistics with Kruskal-Wallis test: $^{***}p < 0.001$.

(F and G) Active Caspase-3 gated on WT-Thy1.1 and Zfx-KO-Thy1.2 tumor cells 5–7 days after anti-PD-L1 treatment. Representative flow cytometry plots on the left (F) and quantification of active Caspase-3 expression on the right (G). Quantification of n = 8–11 mice per group from 2 independent studies. Graph shows the mean, and the error bars indicate SEM. Statistics with one-way ANOVA: $^{***}p < 0.001$, $^{****}p < 0.0001$.

(H) RNA sequencing of WT and Zfx KO MC38 tumor cells from *in vivo* studies. Tumor cells were FACS sorted based on Thy1.1 expressing WT tumor cells and Thy1.2 expressing Zfx KO tumor cells. Hallmark pathway analysis of genes with significant expression changes on the right. Gene set enrichment analysis for apoptosis and TNF signaling pathway on the left.

(I) Heatmap of RNA sequencing data from (H). Expression of selected genes in the apoptosis pathway with *Z* score between -2- and 2-fold change.

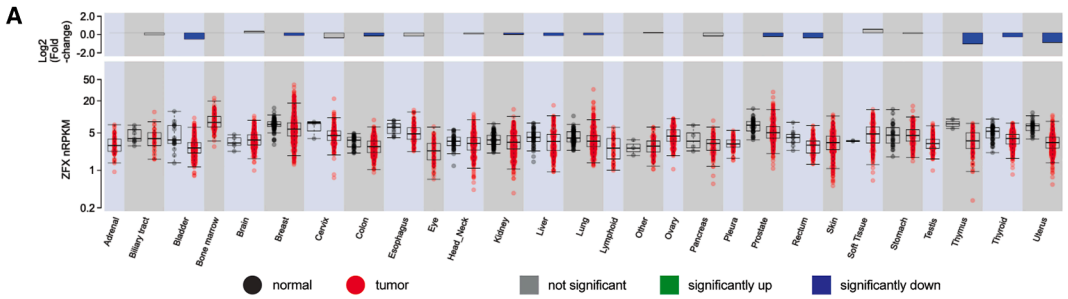

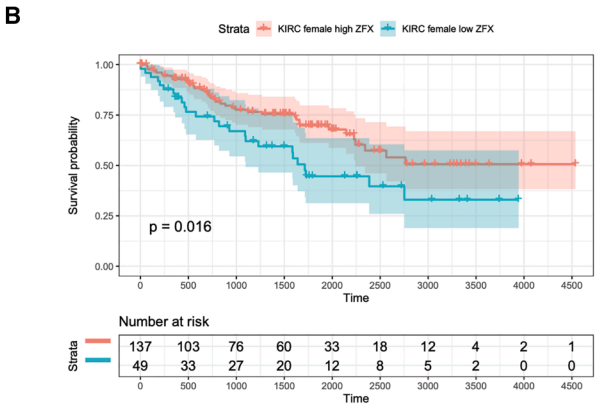

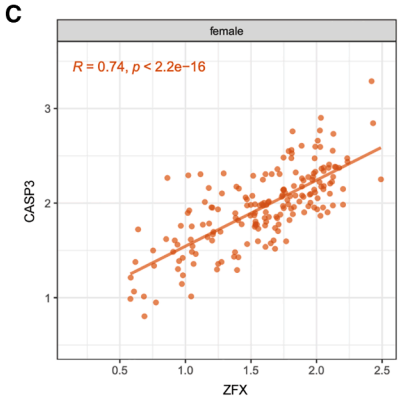

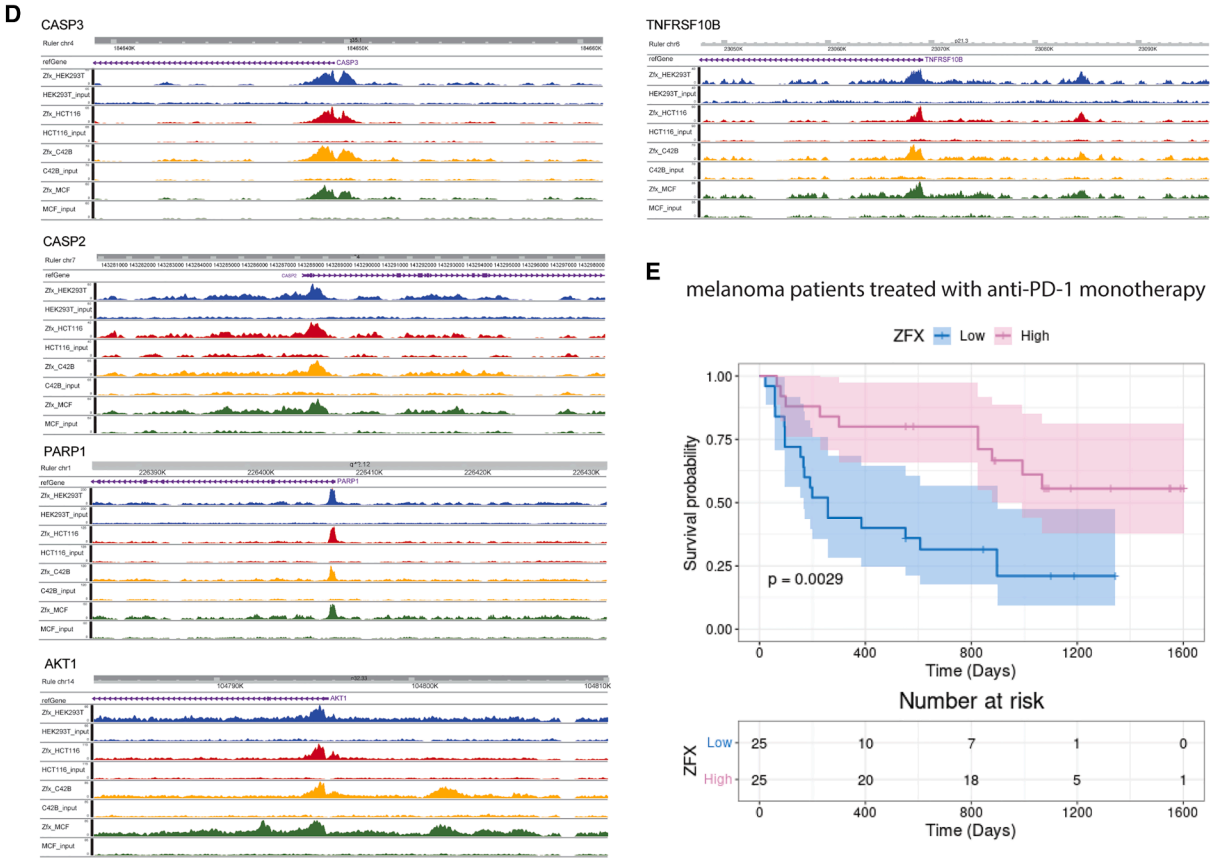

(legend on next page)

Zinc-finger protein X-linked is downregulated in human cancer tissues and regulates CASP3 expression

To extend our study from MC38 tumor cells to relevance in human cancers, we examined the expression levels of *ZFX*. Human *ZFX* is expressed in most tissues. By analyzing RNA expression of *ZFX* across multiple normal and tumor tissues, we found that *ZFX* expression is significantly down-regulated in several tumor tissues, such as bladder, breast, colon, kidney, rectum, thymus, and uterus (Figure 5A). Of note, none of the tumor tissues displayed a significant up-regulation of *ZFX*. Next, we examined whether *ZFX* expression in patients with cancer is correlated with overall survival. Female patients with kidney renal clear cell carcinoma (KIRC) with high *ZFX* expression showed significantly better survival compared to patients with low *ZFX* expression (Figure 5B). In male patients, this difference was not significant (Figure S5C). In addition, we noticed a strong correlation between *ZFX* and *CASP3* expression in female (Figure 5C) and male (Figure S5B) patients with cancer, suggesting a link between *ZFX* and *CASP3* expression in humans that supports our observations in mice. Of note, there is no difference in the overall survival of female and male patients with KIRC (Figure S5A).

Overall, these observations suggest that a similar expression correlation between *ZFX* and *CASP3* exists in humans, as was observed in mice, and that this correlation may drive meaningful differences in survival outcomes.

To investigate the mechanistic role of ZFX in regulating the expression of cell death-associated genes, such as CASP3, we performed chromatin immunoprecipitation sequencing (ChIP-Seq) analysis using publicly available datasets across multiple human cancer cell lines. The ChIP-Seq results demonstrated significant enrichment of ZFX at the promoters of several apoptosis-related genes, including CASP3, CASP2, PARP1, TNFRSF10B, and AKT1 (Figures 5D and S5D). This enrichment was consistently observed across four distinct human cancer cell lines representative of diverse tumor types: kidney (HEK293), colon (HCT116), prostate (C42B), and breast (MCF7).

To further explore the clinical relevance of ZFX, we examined its role in patients with cancer undergoing immunotherapy. Utilizing publicly available datasets (TIGER), we analyzed the correlation between ZFX expression and immunotherapy outcomes. In patients with melanoma treated with anti-PD-1 therapy, high ZFX expression was associated with improved survival, whereas low ZFX expression correlated with poor survival outcomes (Figure 5E). These findings suggest that ZFX may serve as a potential biomarker for predicting immunotherapy efficacy.

In summary, our findings reveal that ZFX plays a critical role in regulating apoptosis-related genes and influencing immunotherapy outcomes. These results suggest that ZFX could serve as both a biomarker for cancer prognosis and a potential therapeutic target to enhance the efficacy of immunotherapy.

DISCUSSION

We utilized a whole-genome loss-of-function genetic screen to identify novel genes that contribute to tumor cell resistance against T cell mediated killing. The deletion of the transcription factor Zfx resulted in killing resistant tumor cells. Mechanistically, this resistance is due to decreased expression of multiple genes associated with cell death signaling pathways, including Casp3. We demonstrated that Zfx KO tumor cells were resistant to T cell-mediated killing *in vitro* and *in vivo* in response to immunotherapy.

MC38 tumor cells have been used in genetic screens for tumor resistance to T cell killing in two earlier studies.[14,16] Our identification of cell death signaling pathways and TNFa was consistent with their findings *in vitro*. However, we found that TNFa does not play a role in the T cell killing of tumor cells *in vivo*. Instead, we identified Perforin/Granzyme B mediated killing as the dominant mechanism in our *in vivo* mouse tumor model. This discrepancy between the *in vitro* vs. *in vivo* mechanisms might not be surprising and could be explained by multiple factors. While we detected high concentrations of TNFa, produced by *in vitro* activated cytotoxic T cells in cell culture, their levels might be lower or less accessible in the *in vivo* tumor model. Moreover, tumor cells grown *in vivo* could be different from tumor cells grown *in vitro* due to different factors or interactions in the tumor microenvironment.

The *in vitro* sensitivity to TNFa-mediated killing seemed to be a unique feature of MC38 tumor cells and did not reproduce to the same extent in other murine tumor cell lines tested. This feature could explain the fact that our screen did not identify members of the antigen presentation complex, such as B2m. As TNFa is a soluble factor and present in high concentrations in the supernatant, tumor cells defective in antigen presentation could still be killed by TNFa in a bystander manner.

We found that expression levels of ZFX are downregulated across multiple human cancer samples compared to healthy tissues, with especially low expression in uterine cancer tissue, indicating that ZFX might have an anti-tumor role when highly expressed. Previous studies with selected human cancer cell lines showed that high *ZFX* expression is correlated with a pro-tumor role, supporting proliferation and tumorigenesis.[21,22] These seemingly contradictory findings could be due to the fact that tumor cell lines are very heterogeneous and represent a large spectrum of differentiation stages, cell morphologies, mutational burden, metabolic states, and many more. While Zfx controls

Figure 5. Role of ZFX in human patients with cancer

(A) ZFX expression levels of healthy and cancer human tissue types. RNA sequencing data from the Cancer Genome Atlas (TCGA). Displayed are normalized reads per kilobase of exon model per million mapped reads (rpkm).

(B) Overall survival of female patients with KIRC with high and low ZFX expression from the Cancer Genome Atlas (TCGA) dataset.

(C) Correlation of ZFX and CASP3 expression in patients with female KIRC.

(D) Traces indicate Zfx ChIPseq reads at the promoters of CASP3, CASP2, PARP1, AKT1, and TNFRSF10B in HEK293T (blue), HCT116 (red), C42B (orange), and MCF cell lines (green). Location of coding region is shown in purple at the top of each plot.

(E) Survival of patients with melanoma treated with anti-PD-1 monotherapy stratified by high and low ZFX expression from the TIGER (Tumor Immunotherapy Gene Expression Resource) database.

cell-renewal of embryonic and hematopoietic stem cells, it is dispensable for differentiated cells.[23] This could explain why some tumor cell lines are dependent on ZFX for their proliferation and survival, while others are more differentiated and proliferate independently of *ZFX*.

Female patients with KIRC with high ZFX expression exhibit significantly enhanced overall survival; however, this difference is not observed in male patients. It is interesting to note that there is a *ZFY* gene on the Y chromosome in males, which is a member of the C_2H_2 zinc finger family comprising *ZFX*, *ZFY,* and *ZNF11*. *ZFX* and *ZFY* are closely related and encode almost identical proteins, with an overall similarity of 96% and a similarity of 99% in the zinc finger domains.[24] ChIP-sequencing has revealed a high similarity within the binding patterns of *ZFX* and ZFY throughout the human genome.[25] Based on these observations, we speculate that *ZFY* might perform functions similar to ZFX and might be able to compensate for the phenotype in male patients with KIRC with low *ZFX* expression. This could result in a smaller difference in overall survival between males with high and low *ZFX* expression in patients with KIRC. Whether *ZFY* regulates the expression of Casp3 and other members of the cell death pathway remains to be elucidated. Similarly, the murine MC38 tumor cell line, derived from a female C57BL/6 mouse, may explain our identification of Zfx in the screen, as Zfy was not present to compensate for Zfx, which could have occurred in a male-derived tumor cell line.

Casp3 is not only associated with TNFa-mediated killing, but also two additional major cytotoxicity pathways, namely Perforin/Granzyme B and FasL-mediated apoptosis.[26] We demonstrated that Zfx regulates the expression of Casp3 and thus expression levels of Zfx might predict cell death resistance to cancer therapy and could be used as a potential biomarker for immunotherapy treatments. In addition, enhancing Zfx expression could be a new approach to boost immunotherapy.

RESOURCE AVAILABILITY

Lead contact

Further information and requests for resources and reagents should be directed to and will be fulfilled by the lead contact, Ulrike Kaufmann (kaufmann.ulrike@gene.com).

Materials availability

This study did not generate new unique reagents.

Data and code availability

- RNAseq data is deposited under Gene Expression Omnibus (GEO) accession number: GSE276964 for the *in vitro* and GSE276965 for the *in vivo* RNAseq data, respectively.
- Original western blot images have been deposited at Mendeley at https://doi.org/10.17632/ykfjmd8nb6.1 and are publicly available as of the date of publication.
- This article does not report original code.
- Any additional information required to reanalyze the data reported in this article is available from the lead contact upon request.

ACKNOWLEDGMENTS

We thank the *In vivo* Cell Culture lab, the Next Generation Sequencing Lab, the FACS Core lab, Laboratory Animal Resources, and the In Vivo Pharmacology team for their support. Illustrations were generated with BioRender.

AUTHOR CONTRIBUTIONS

U.K. and H.H. conceived of the project with assistance from S.M. and M.C.; U.K. and H.H. designed the project and wrote the article with assistance from D.N.; U.K. designed experiments; U.K., J.W., M.G.C., E.C., and E.W. performed experiments and acquired data; U.K., M.G.C., JP.F., S.M., D.N., R.R., B.H., Y.L., S.M., and M.C. performed CRISPR screen, RNASeq analysis and visualization, and bioinformatics.

DECLARATION OF INTERESTS

All authors are or were employees and shareholders of Genentech, a member of the Roche group, which develops and markets drugs for profit.

STAR★METHODS

Detailed methods are provided in the online version of this paper and include the following:

- KEY RESOURCES TABLE
- METHOD DETAILS
  - Cell lines
  - Cell engineering
  - Whole-genome CRISPR-Cas9 screen
  - Mice and tumor studies
  - Tumor processing
  - Generation of cytotoxic T cells
  - Cytotoxicity assay and competition assay
  - Flow cytometry
  - Immunoblotting
  - RNA sequencing
  - Real-time quantitative PCR assays
  - Proliferation assay
  - Enzyme-linked immunosorbent assay (ELISA)
  - ChIP-seq data analysis
  - Data availability
- QUANTIFICATION AND STATISTICAL ANALYSIS

SUPPLEMENTAL INFORMATION

Supplemental information can be found online at https://doi.org/10.1016/j.isci.2025.113842.

Received: September 22, 2025
Revised: October 18, 2025
Accepted: October 18, 2025
Published: October 23, 2025

REFERENCES

1. Chen, D.S., and Mellman, I. (2013). Oncology Meets Immunology: The Cancer-Immunity Cycle. Immunity *39*, 1–10.
2. Leach, D.R., Krummel, M.F., and Allison, J.P. (1996). Enhancement of Antitumor Immunity by CTLA-4 Blockade. Science *271*, 1734–1736.
3. Freeman, G.J., Long, A.J., Iwai, Y., Bourque, K., Chernova, T., Nishimura, H., Fitz, L.J., Malenkovich, N., Okazaki, T., Byrne, M.C., et al. (2000). Engagement of the Pd-1 Immunoinhibitory Receptor by a Novel B7 Family Member Leads to Negative Regulation of Lymphocyte Activation. J. Exp. Med. *192*, 1027–1034.
4. Barber, D.L., Wherry, E.J., Masopust, D., Zhu, B., Allison, J.P., Sharpe, A.H., Freeman, G.J., and Ahmed, R. (2006). Restoring function in exhausted CD8 T cells during chronic viral infection. Nature *439*, 682–687.
5. Ahmadzadeh, M., Johnson, L.A., Heemskerk, B., Wunderlich, J.R., Dudley, M.E., White, D.E., and Rosenberg, S.A. (2009). Tumor antigen–specific CD8 T cells infiltrating the tumor express high levels of PD-1 and are functionally impaired. Blood *114*, 1537–1544.

6. Topalian, S.L., Hodi, F.S., Brahmer, J.R., Gettinger, S.N., Smith, D.C., McDermott, D.F., Powderly, J.D., Carvajal, R.D., Sosman, J.A., Atkins, M.B., et al. (2012). Safety, Activity, and Immune Correlates of Anti–PD-1 Antibody in Cancer. N. Engl. J. Med. *366*, 2443–2454.

7. Reck, M., Rodríguez-Abreu, D., Robinson, A.G., Hui, R., Csőszi, T., Fülöp, A., Gottfried, M., Peled, N., Tafreshi, A., Cuffe, S., et al. (2016). Pembrolizumab versus Chemotherapy for PD-L1–Positive Non–Small-Cell Lung Cancer. N. Engl. J. Med. *375*, 1823–1833.

8. Wolchok, J.D., Chiarion-Sileni, V., Gonzalez, R., Rutkowski, P., Grob, J.J., Cowey, C.L., Lao, C.D., Wagstaff, J., Schadendorf, D., Ferrucci, P.F., et al. (2017). Overall Survival with Combined Nivolumab and Ipilimumab in Advanced Melanoma. N. Engl. J. Med. *377*, 1345–1356.

9. Pitt, J.M., Vétizou, M., Daillère, R., Roberti, M.P., Yamazaki, T., Routy, B., Lepage, P., Boneca, I.G., Chamaillard, M., Kroemer, G., and Zitvogel, L. (2016). Resistance Mechanisms to Immune-Checkpoint Blockade in Cancer: Tumor-Intrinsic and -Extrinsic Factors. Immunity *44*, 1255–1269.

10. O'Donnell, J.S., Smyth, M.J., and Teng, M.W.L. (2016). Acquired resistance to anti-PD1 therapy: checkmate to checkpoint blockade? Genome Med. *8*, 111.

11. Bellone, M., and Elia, A.R. (2017). Constitutive and acquired mechanisms of resistance to immune checkpoint blockade in human cancer. Cytokine Growth Factor Rev. *36*, 17–24.

12. Patel, S.J., Sanjana, N.E., Kishton, R.J., Eidizadeh, A., Vodnala, S.K., Cam, M., Gartner, J.J., Jia, L., Steinberg, S.M., Yamamoto, T.N., et al. (2017). Identification of essential genes for cancer immunotherapy. Nature *548*, 537–542.

13. Pan, D., Kobayashi, A., Jiang, P., Ferrari de Andrade, L., Tay, R.E., Luoma, A.M., Tsoucas, D., Qiu, X., Lim, K., Rao, P., et al. (2018). A major chromatin regulator determines resistance of tumor cells to T cell–mediated killing. Science *359*, 770–775.

14. Kearney, C.J., Vervoort, S.J., Hogg, S.J., Ramsbottom, K.M., Freeman, A.J., Lalaoui, N., Pijpers, L., Michie, J., Brown, K.K., Knight, D.A., et al. (2018). Tumor immune evasion arises through loss of TNF sensitivity. Sci. Immunol. *3*, eaar3451.

15. Vredevoogd, D.W., Kuilman, T., Ligtenberg, M.A., Boshuizen, J., Stecker, K.E., de Bruijn, B., Krijgsman, O., Huang, X., Kenski, J.C.N., Lacroix, R., et al. (2019). Augmenting Immunotherapy Impact by Lowering Tumor TNF Cytotoxicity Threshold. Cell *178*, 585–599.e15.

16. Lawson, K.A., Sousa, C.M., Zhang, X., Kim, E., Akthar, R., Caumanns, J.J., Yao, Y., Mikolajewicz, N., Ross, C., Brown, K.R., et al. (2020). Functional genomic landscape of cancer-intrinsic evasion of killing by T cells. Nature *586*, 120–126.

17. Juneja, V.R., McGuire, K.A., Manguso, R.T., LaFleur, M.W., Collins, N., Haining, W.N., Freeman, G.J., and Sharpe, A.H. (2017). PD-L1 on tumor cells is sufficient for immune evasion in immunogenic tumors and inhibits CD8 T cell cytotoxicity. J. Exp. Med. *214*, 895–904.

18. Restifo, N.P., Marincola, F.M., Kawakami, Y., Taubenberger, J., Yannelli, J.R., and Rosenberg, S.A. (1996). Loss of Functional Beta2-Microglobulin in Metastatic Melanomas From Five Patients Receiving Immunotherapy. J. Natl. Cancer Inst. *88*, 100–108.

19. Liberzon, A., Birger, C., Thorvaldsdóttir, H., Ghandi, M., Mesirov, J.P., and Tamayo, P. (2015). The Molecular Signatures Database Hallmark Gene Set Collection. Cell Syst. *1*, 417–425.

20. Behan, J.W., Ehsanipour, E.A., Sheng, X., Pramanik, R., Wang, X., Hsieh, Y.T., Kim, Y.M., and Mittelman, S.D. (2013). Activation of adipose tissue macrophages in obese mice does not require lymphocytes. Obesity *21*, 1380–1388.

21. Wu, S., Lao, X.Y., Sun, T.T., Ren, L.L., Kong, X., Wang, J.L., Wang, Y.C., Du, W., Yu, Y.N., Weng, Y.R., et al. (2013). Knockdown of ZFX inhibits gastric cancer cell growth *in vitro* and *in vivo* via downregulating the ERK-MAPK pathway. Cancer Lett. *337*, 293–300.

22. Rhie, S.K., Yao, L., Luo, Z., Witt, H., Schreiner, S., Guo, Y., Perez, A.A., and Farnham, P.J. (2018). ZFX acts as a transcriptional activator in multiple types of human tumors by binding downstream from transcription start sites at the majority of CpG island promoters. Genome Res. *28*, 310–320.

23. Galan-Caridad, J.M., Harel, S., Arenzana, T.L., Hou, Z.E., Doetsch, F.K., Mirny, L.A., and Reizis, B. (2007). Zfx Controls the Self-Renewal of Embryonic and Hematopoietic Stem Cells. Cell *129*, 345–357.

24. North, M., Sargent, C., O'Brien, J., Taylor, K., Wolfe, J., Affara, N.A., and Ferguson-Smith, M.A. (1991). Comparison of ZFY and ZFX gene structure and analysis of alternative 3′ untranslated regions of ZFY. Nucleic Acids Res. *19*, 2579–2586.

25. Ni, W., Perez, A.A., Schreiner, S., Nicolet, C.M., and Farnham, P.J. (2020). Characterization of the ZFX family of transcription factors that bind downstream of the start site of CpG island promoters. Nucleic Acids Res. *48*, 5986–6000.

26. Du, W., and Cao, X. (2018). Cytotoxic Pathways in Allogeneic Hematopoietic Cell Transplantation. Front. Immunol. *9*, 2979.

27. Hoberecht, L., Perampalam, P., Lun, A., and Fortin, J.-P. (2022). A comprehensive Bioconductor ecosystem for the design of CRISPR guide RNAs across nucleases and technologies. Nat. Commun. *13*, 6568.

28. Huber, W., Carey, V.J., Gentleman, R., Anders, S., Carlson, M., Carvalho, B.S., Bravo, H.C., Davis, S., Gatto, L., Girke, T., et al. (2015). Orchestrating high-throughput genomic analysis with Bioconductor. Nat Methods *12*, 115–121.

29. Robinson, M.D., and Oshlack, A. (2010). A scaling normalization method for differential expression analysis of RNA-seq data. Genome Biol. *11*, R25.

30. Hart, T., Brown, K.R., Sircoulomb, F., Rottapel, R., and Moffat, J. (2014). Measuring error rates in genomic perturbation screens: gold standards for human functional genomics. Mol. Syst. Biol. *10*, 733.

31. Law, C.W., Chen, Y., Shi, W., and Smyth, G.K. (2014). voom: precision weights unlock linear model analysis tools for RNA-seq read counts. Genome Biol. *15*, R29.

32. Simes, R.J. (1986). An Improved Bonferroni Procedure for Multiple Tests of Significance. Biometrika *73*, 751–754.

33. Pau, G., and Reeder, J. (2012). HTSeqGenie: a NGS analysis pipeline. R package version 3.14.0.

34. Wu, T.D., and Nacu, S. (2010). Fast and SNP-tolerant detection of complex variants and splicing in short reads. Bioinformatics *26*, 873–881.

35. Robinson, M.D., McCarthy, D.J., and Smyth, G.K. (2010). edgeR: a Bioconductor package for differential expression analysis of digital gene expression data. Bioinformatics *26*, 139–140.

36. Ritchie, M.E., Phipson, B., Wu, D., Hu, Y., Law, C.W., Shi, W., and Smyth, G.K. (2015). limma powers differential expression analyses for RNA-sequencing and microarray studies. Nucleic Acids Res. *43*, e47.

37. Liberzon, A., Subramanian, A., Pinchback, R., Thorvaldsdóttir, H., Tamayo, P., and Mesirov, J.P. (2011). Molecular signatures database (MSigDB) 3.0. Bioinformatics *27*, 1739–1740.

38. Subramanian, A., Tamayo, P., Mootha, V.K., Mukherjee, S., Ebert, B.L., Gillette, M.A., Paulovich, A., Pomeroy, S.L., Golub, T.R., Lander, E.S., and Mesirov, J.P. (2005). Gene set enrichment analysis: A knowledge-based approach for interpreting genome-wide expression profiles. Proc. Natl. Acad. Sci. USA *102*, 15545–15550.

STAR★METHODS

KEY RESOURCES TABLE

REAGENT or RESOURCE	SOURCE	IDENTIFIER
Antibodies		
Granzyme B APC (clone:GB12)	Life Technologies	MHGB05; RRID: AB_10373420
IFNg PerCP-Cy5.5 (clone: XMG1.2)	eBiosciences	45-7311-82; RRID: AB_1107020
CD8 APC-R700 (clone: 53-6.7)	BD Biosciences	564983; RRID: AB_2739032
CD107a FITC (clone: 1D4B)	Biolegend	121606; RRID: AB_572007
TNFa BV510 (clone: MP6-XT22)	Biolegend	506339; RRID: AB_2563127
Thy1.1 SB436 (clone: A152)	eBiosciences	62-0900-82; RRID: AB_2744782
Thy1.1 FITC (clone: HIS51)	eBiosciences	11090081; RRID: AB_465151
Thy1.2 BUV661 (clone: 30-H12)	BD Biosciences	741458; RRID: AB_2870927
Thy1.2 PE (clone: 30-H12)	eBiosciences	12-0903-83; RRID: AB_465780
H2Kb-H2Db BV421 (clone 28-8-6)	BD Biosciences	744664; RRID: AB_2742402
CD45 BV786 (clone: 30-F11)	Biolegend	103149; RRID: AB_2564590
CD3 BV737 (clone: 145-2C11)	BD Biosciences	741788; RRID: AB_2871136
CD4 PE-CF594 (clone: RM4-5)	BD Biosciences	562285; RRID: AB_11154410
PD-1 PerCP-Cy5.5 (clone: 29F.1A12)	Biolegend	135208; RRID: AB_2159184
Tim3 BV605 (clone: RMT3-23)	Biolegend	119721; RRID: AB_2616907
CD62L BV421 (MEL-14)	BD Biosciences	562910; RRID: AB_2737885
CD44 BV510	Biolegend	103044; RRID: AB_2650923
CD11b BUV396 (clone: M1/70)	BD Biosciences	563553; RRID: AB_3704601
CD19 BUV396 (clone: 1D3)	BD Biosciences	563557; RRID: AB_2722495
F4/80 BUV396 (clone: T45-2342)	BD Biosciences	565614; RRID: AB_2739304
I-A/I-E BUV396 (clone: 2G9)	BD Biosciences	743876; RRID: AB_2741827
γδ T Cell Receptor BUV396 (clone: GL3)	BD Biosciences	744118; RRID: AB_2742008
Caspase-3 (clone: 5A1E)	Cell Signaling	9664; RRID: AB_2070042
PD-L1 (clone: 6E11)	Genentech	
Neutralizing anti-TNFa	Biolegend	506325; RRID: AB_2204355
Chemicals, peptides, and recombinant proteins		
$OVA_{257-264}$ (SIINFEKL) peptide	AnaSpec	AS-60193-1
human IL-2	PeproTech	10779-570
murine TNFa	PeproTech	315-01A-50ug
Critical commercial assays		
CellTiterGlo	Promega	G7571
RNA extraction (RNeasy)	Qiagen	80204
TNFa Instant ELISA Kit	Invitrogen	BMS607-2INST
Deposited data		
RNAseq *in vitro*		GSE276964
RNAseq *in vivo*		GSE276965
Experimental models: Cell lines		
CT26	ATCC	
HEPA1-6	ATCC	
TC-1	ATCC	
TRMAP-C1	ATCC	
MC-38	Genentech	
E0771	CH3 BioSystems	
51BLim10	UC Berkeley	

(*Continued on next page*)

Continued

REAGENT or RESOURCE	SOURCE	IDENTIFIER
Experimental models: Organisms/strains		
C57BL/6	Jackson Laboratory	000664
C57BL/6 Perforin KO	Jackson Laboratory	002407
NSG	Jackson Laboratory	005557
Oligonucleotides		
Casp3	TaqMan Thermo Fisher	Mm01195085_m1
Casp8	TaqMan Thermo Fisher	Mm01255716_m1
Tnfrsf1a	TaqMan Thermo Fisher	Mm00441883_g1
Gapdh	TaqMan Thermo Fisher	Mm99999915_g1
Software and algorithms		
FlowJo 10.8.1	BD Biosciences	
BioRender	BioRender	
GraphPad Prism 10.5.0	GraphPad Software	

METHOD DETAILS

Cell lines

Murine tumor cell lines CT26, HEPA1-6, TC-1, TRMAP-C1 (all ATCC), MC38 (Genentech), E0771 (CH3 BioSystems) and 51BLim10 (UC Berkeley) were cultured in RPMI-1640 medium containing 10% heat-inactivated fetal bovine serum (FBS) and 2 mM L-glutamine (Gibco). Cell lines were kept at low passages and tested negative for *Mycoplasma*.

Cell engineering

The piggybac transposase system was used for stable integration of expression plasmids. All constructs were purchases from GenScript. Cells were transfected with Lipofectamine 3000 (Invitrogen) following manufacturer's instructions and piggybac plasmids were added along with the pBO transposase plasmid. Cells were allowed to express the constructs and either selected with antibiotics (2 μg/ml blasticidin, 4 μg/ml puromycin or 100 μg/ml zeocin) or FACS sorted for protein expression to obtain pure populations.

To delete genes of interest from tumor cells, Cas9 ribonucleoprotein (RNP) complexes were transfected into cells using CRISPRMAX lipofectamine (Invitrogen) according to manufacturer's instructions. All sgRNAs were purchased from IDT and Cas9 proteins from Sigma-Aldrich or Invitrogen.

Genotyping of KO tumor cells was done with next generation sequencing (NGS). First, DNA was isolated with DNeasy Blood and Tissue kit (QIAGEN). Followed by PCR amplification of region of interest. PCR products were cleaned with QIAquick PCR purification kit (QIAGEN) and analyzed by NGS.

Whole-genome CRISPR-Cas9 screen

Sample collection

Cells were infected in triplicate samples separately with 8 sgRNA library pools (Supplementary file 1). Each sgRNA library pool was designed to target each gene with 8 sgRNAs when possible, and the 8 sgRNA library pools together target the entire set of mouse protein-coding genes. For the three replicates, genomic DNA was isolated and integrated sgRNAs were amplified by PCR for cells harvested at:

- 2 days after sgRNA infection for the first two sgRNA pools, and 3 days after sgRNA infection for the remaining two sgRNA pools. Those samples are labeled as Reference samples.
- Just before the first round of T cell-mediated killing (6 days after infection). Those samples are labeled as Input samples.
- 3-4 days after the second and third round of killing (13 and 20 days after infection, respectively) for the first two sgRNA pools, or the third and fourth round of killing (20 and 41 days after infection) for the remaining two sgRNA pools.

for a total of 48 amplicon samples.

Briefly, an amount of genomic DNA to maintain representation was mixed with Phusion High-Fidelity PCR Master Mix with GC Buffer (NEB, M0531L), forward (TCTTGTGGAAAGGACGAGGTACCG) and reverse (TCTACTATTCTTTCCCCTGCACTGT) primers, representing complimentary guide flanking sequences in multiple 100 ul reactions. Adapter ligation and indexing PCR was performed on these amplicons using KAPA HTP Library Preparation Kit (Kapa biosystems, K8234) for multiplexing and sequencing on an Illumina HiSeq4000 platform.

Read alignment of the pooled amplicon sequencing samples

Amplicons were sequenced on an Illumina HiSeq 4000 instrument, using 50bp single-end reads.

The average Phred quality score was above 38 for all 48 samples, and all 48 samples had at least 40M reads. Read sequences were searched for an exact match of any one of the gRNA barcode sequences, using the screenCounter R package available in the crisprVerse.[27] The number of reads matched to each guide in each sample was used to obtain a guide-by-sample count matrix for further analysis. We combined counts across sgRNA library pools, for a total of 12 samples for further analysis (3 replicates across 4 conditions). Counts within a replicate and condition were adjusted for library size before merging.

Statistical analysis

The raw count data were stored in a standard Bioconductor Summarized Experiment object.[28] Normalization is needed to adjust for the difference in sequencing depth between samples, and to account for potential compositional biases due to the competitive nature of pooled genetic screening.

We estimated normalization factors for each sample by applying the TMM method[29] on the count data for gRNAs targeting a gold-standard set of non-essential genes (obtained from[30]).

We performed a differential abundance analysis at the gRNA level using the popular limma-voom approach.[31] Specifically, we fitted a linear model to the log-CPM values for each gRNA, using voom-derived observation and quality weights. We performed robust empirical Bayes shrinkage to obtain shrunken variance estimates for each gRNA, and we used moderated F-tests to compute p-values for each of the two-group comparisons of interest. To control the FDR in each comparison, we applied the standard Benjamini-Hochberg method to obtain an adjusted p-value for each gRNA.

We then used the gRNA-level statistics to obtain gene-level summaries using two complementary statistical approaches. The first approach was to aggregate gRNA statistics by reusing the ''fry'' gene-set enrichment analysis method implemented in limma, and considering gRNAs targeting a given gene as a ''gene set''. This allows the detection of genes that are consistently enriched or depleted for the majority of the gRNAs designed for each gene. The second approach uses Simes' method[32] to obtain a combined p-value for each gene based on the p-values for all associated gRNAs. This allows the detection of differentially-abundant genes in cases where only a small proportion of the gRNAs show a strong signal. Gene-level p-values were corrected for multiple comparisons using the Benjamini-Hochberg method.

Mice and tumor studies

WT C57BL/6 or Perforin KO (002407) mice were from Taconic Biosciences and the Jackson Laboratory. All mice were housed in individually ventilated cages and acclimated to study conditions for at least 7 days.

For syngeneic tumor studies, female mice 6-10-week-old were inoculated subcutaneously in the right flank with 1 x 10^6 tumor cells resuspended in 50% Hank's balanced salt solution (HBSS) and 50% Matrigel (Corning). Tumor volumes were monitored twice a week until they became established and reached a volume of 120-200 mm^3. Mice were randomized into treatment groups and treated with either isotype control antibody gp120 mIgG1 or anti-PD-L1 mIgG1 (clone 6E11) at 10 mg/kg intravenously for the first dose followed by 5 mg/kg intraperitoneally two times per week. Antibodies were diluted in histidine buffer (20 mmol/L histidine acetate, 240 mmol/L sucrose and 0.02% polysorbate 20, pH 5.5). Tumor volumes were measured in two dimensions: length and width. Tumor volume was calculated using the following formula: tumor volume (mm^3) = (length x $width^2$) x 0.5.

All animal studies were approved by the Genentech Institutional Animal Care and Use Committee following relevant ethical regulations.

Tumor processing

Tumors were collected in RPMI-1640, minced and enzymatically digested with 0.2 mg/ml Collagenase P (Roche), 0.8 mg/ml Dispase (Life Technologies) and 0.1 mg/ml DNase I (Roche) in RPMI-1640 at 37°C for 45 min. After tumor digestion cells were washed with RPMI-1640 containing 10% FBS and filtered with a 70-μm cell strainer.

Generation of cytotoxic T cells

Splenocytes were isolated from OT-I mice, single cell suspensions were prepared and cells were stimulated with 10 nM $OVA_{257-264}$ (SIINFEKL) peptide (AnaSpec) in T cell medium (RPMI-1640 with 10% FBS, 2 mM L-glutamine and 50 μM β-mercaptoethanol). After 2 days of stimulation, T cells were expanded in T cell medium containing 50 U recombinant human IL-2 (PeproTech) for 3 days. T cells were used for cytotoxicity assays on day 5.

Cytotoxicity assay and competition assay

T cell-mediated cytotoxicity assays: Tumor cells were loaded with 1 μM SIINFEKL peptide (AnaSpec) and co-cultured with activated OT-I T cells at a 1:1 ratio for 5-24 h. Tumor cells without peptide loading and tumor cells without addition of T cells were used as control for normalization. After the co-culture, T cells were washed out with PBS and remaining tumor cells were analyzed for their viability with CellTiter-Glo assay (Promega) following manufacturer's instructions.

For competition assays a similar protocol was used with mixtures of tumor cells engineered to express Thy1.1 and Thy1.2 to be able to distinguish them. Flow cytometry analysis was performed before and after the killing assay to evaluate changes in tumor cell ratios.

TNFa-mediated cytotoxicity assays: Tumor cells were treated with dose titrations of recombinant murine TNFa (Peprotech) ranging from 0-50 ng/ml for 5-24 h. Viability of tumor cells was measured with CellTiter-Glo assay (Promega) following manufacturer's instructions.

Neutralizing anti-TNFa antibody (BioLegend) at a concentration of 50 μg/ml was used to block TNFa produced by activated T cells or recombinant murine protein.

Flow cytometry

Single cell suspensions were kept in FACS buffer and were stained with the following fluorochrome-conjugated antibodies against mouse antigens: CD45 (30-F11, BD), CD11b (M1/70, BD), CD19 (1D3, BD), F4/80 (T45-2342, BD), I-A/I-E (2G9, BD), gdTCR (GL3, BD), CD3 (145-2C11, BD), CD4 (RM4-5, BD), CD8 (53-6.7, BD), PD-1 (29F.1A12, BioLegend), Tim3 (RMT3-23, BioLegend), Thy1.1 (HIS51, eBiosciences), Thy1.2 (30-H12, eBiosciences) and CD107a (1D4B, BD). For intracellular staining cells were fixed and permeabilized with IC Fixation Buffer (eBiosiences) and stained for intracellular antigens: TNFa (MP6-XT22, BioLegend), IFNg (XMG1.2, eBiosciences), Granzyme B (GB12, LifeTechnologies). Cell viability was determined using fixable viability dye eFluor780 from eBiosciences. Fc-receptors were blocked with anti-CD16/CD32 antibodies (BD) for 10 min before staining with other antibodies. For cytokine staining cells were treated with cell stimulation cocktail with protein transport inhibitor (eBiosciences) for 4 h before antibody staining. Flow cytometric data were acquired using FACSymphony (BD) and data were analyzed with FlowJo software 10.8.1 (BD).

Viable tumor cells were sorted based on Thy1.1 and Thy1.2 expression and negative staining for CD45 using a FACS Aria Fusion cell sorter (BD).

Immunoblotting

To analyze protein content in tumor cells cultured *in vitro* or collected *ex vivo*, cells were washed with PBS and lysed with cell lysis buffer (Invitrogen) containing protease and phosphatase inhibitor cocktail (Thermo Scientific) for 30 minutes on ice. Supernatants were collected after centrifugation at 14000 rpm for 4 minutes. Protein concentrations were measured with Pierce BCA protein assay kit (Thermo Scientific) according to manufacturer's instructions. 25 μg protein were combined with 4x NuPage LDS sample buffer (Thermo Scientific) and 10x NuPage sample reducing agent (Thermo Scientific), heated at 70°C for 5 minutes and run on NuPage 4 to 12% Bis Tris 1mm Midi Protein Gel (Invitrogen). Proteins were transferred to nitrocellulose membranes (iBlot 2 Transfer Stacks, Invitrogen), blocked with TBS blocking buffer (Licor) and stained with relevant antibodies. Fluorescence signals were captured with Odyssey (Licor). The following antibodies were used: Caspase-3 full length and cleaved Caspase-3 (5A1E) (Cell Signaling).

RNA sequencing

RNA was isolated from *in vitro* cultured tumor cells or FACS sorted *ex vivo* tumor cells with RNeasy (QIAGEN) following manufacturer's instructions, including DNase treatment steps. Quality control was performed with NanoDrop (Thermo Scientific) and 1 μg RNA was used for RNA sequencing.

RNA extraction

Total RNA was extracted from sorted tumor cells using the Qiagen All Prep nucleic isolation kit (Qiagen, Inc.; catalog number 80204, Valencia, CA) as per the manufacturer's protocol, including the on-column DNase digestion. Total RNA was quantified with Qubit RNA HS Assay Kit (Thermo Fisher Scientific catalog#: Q32852) and quality was assessed using RNA ScreenTape on 4200 TapeStation (Agilent Technologies catalog#: 5067-5576).

Library preparation

An input of 100-1000 nanogram of total RNA was used to make sequencing libraries by Trueseq Stranded mRNA kit (Illumina catalog#: 20020594). Libraries were quantified with Qubit dsDNA HS Assay Kit (Thermo Fisher Scientific catalog#: Q32851) and the average library size was determined using D1000 ScreenTape on 4200 TapeStation (Agilent Technologies catalog#: 5067-5582). Libraries were pooled and sequenced on NovaSeq 6000 (Illumina) to generate 30 million single-end 50-base pair reads for each sample.

RNA sequencing data analysis

RNA-sequencing data for TCGA were obtained from the National Cancer Institute Genomic Data Commons (https://gdc.cancer.gov).

Sequencing data were processed using HTSeqGenie[33] as follows: first, reads with low nucleotide qualities (70% of bases with quality <23) or rRNA and adapter contamination were removed; subsequently reads that passed QC were aligned to the reference genome GRCh38 usingGSNAP.[34] Log2 transformed counts per million (logCPM) were calculated using egdeR functionality.[35] Subsequently, voom/limma using robust empirical Bayes and array weights, was used for differential gene expression analysis, comparing baseline gene expression in the wildtype condition to transcriptomes in the ZFX knockout[31,36] and MSigDB's Hallmark collection.[19,37,38]

For testing associations of ZFX expression with survival in TCGA's KIRC cohort, patients were grouped based on median ZFX expression (low < median expression). Cox proportional hazard regression models were fit, using survival as response and ZFX status as term, comparing ZFX high to low tumors. This was done in male and female patients separately to account for the higher expression of ZFX in female patients. We also fit a Cox proportional hazard regression model comparing survival between male and female patients (regardless of ZFX expression). Reported p values were determined using Wald tests.

To assess a putative correlation between ZFX and CASP3 expression in female and male KIRC patients, respectively, Pearson correlation coefficients and p-values were calculated.

TCGA gene expression analysis

RNA-sequencing data for TCGA were obtained from the National Cancer Institute Genomic Data Commons (https://gdc.cancer.gov). The data was processed using HTSeqGenie[33] as follows: first, reads with low nucleotide qualities (70% of bases with quality <23) or rRNA and adapter contamination were removed; subsequently reads that passed were aligned to the reference genome GRCh38 using GSNAP.[26] Alignments of the reads that were reported by GSNAP as ''uniquely mapping'' were used for subsequent analysis. Gene expression was quantified as Reads Per Kilobase of exon model per Million mapped reads normalized by size factor (nRPKM), defined as number of reads aligning to a gene in a sample / (total number of uniquely mapped reads for that sample x gene length x size factor).

Real-time quantitative PCR assays

RNA was purified using RNeasy kit (QIAGEN), which includes a DNase digestion step. Mouse transcripts were quantified from 10 ng RNA input using TaqMan RNA-to-CT reagents (Thermo Fisher) with ViiA7 real-time PCR system (Thermo Fisher). Ct values were normalized to the housekeeping gene Gapdh and $2^{-\Delta\Delta Ct}$ calculations were used to determine RNA expression levels. The following primers were used: Casp3 (Mm01195085_m1), Casp8 (Mm01255716_m1), Tnfrsf1a (Mm00441883_g1) and Gapdh (Mm99999915_g1) from TaqMan Thermo Fisher.

Proliferation assay

For *in vitro* cell proliferation assays 500 cells were plated per well of 96-well-plates in cell culture medium. Number of viable cells was determined every day for 5 consecutive days with CellTiter-Glo assay (Promega) following manufacturer's instructions.

Enzyme-linked immunosorbent assay (ELISA)

Supernatant of co-cultures of peptide loaded tumor cells with activated antigen-specific T cells were collected after 5 h. TNFa levels were measured using Instant ELISA Kit from Invitrogen.

ChIP-seq data analysis

ZFX ChIPseq data was downloaded from GEO (GSE102616). The raw FASTQ files were aligned to the human reference genome (GRCh38) using BWA (version 0.7.12-r1039). Reads that mapped uniquely to the genome and aligned with no more than 2 mismatches were used for downstream analyses. WashU epigenome browser was used to plot the locus specific ChIP-seq read enrichment.

Data availability

RNAseq data is deposited under Gene Expression Omnibus (GEO) accession number: GSE276964 for the *in vitro* and GSE276965 for the *in vivo* RNAseq data respectively.

QUANTIFICATION AND STATISTICAL ANALYSIS

Statistical analyses were performed using GraphPad Prism, and the statistical details of the experiments are provided in the figure legends. Error bars represent the SEM of typically three replicates, unless otherwise specified. Statistical tests, including Welch's t test, unpaired t test, one-way ANOVA, Welch ANOVA, or Kruskal–Wallis test, were conducted as indicated in the figure legends. Significance levels are denoted as follows: $p < 0.05$ (*), $p < 0.005$ (**), $p < 0.0005$ (***), and $p < 0.0001$ (****).